



Published in final edited form as:

*J Cell Mol Med.* 2009 September ; 13(9B): 3720–3729. doi:10.1111/j.1582-4934.2009.00785.x.

## VEGFR2+PDGFR $\beta$ + circulating precursor cells participate in capillary restoration after hyperoxia acute lung injury (HALI)

Rosemary Jones<sup>1</sup>, Diane E. Capen<sup>1</sup>, Margaretha Jacobson<sup>1</sup>, Kenneth S. Cohen<sup>2</sup>, David T. Scadden<sup>2</sup>, and Dan G. Duda<sup>3</sup>

<sup>1</sup>Department of Anesthesia and Critical Care, Massachusetts General Hospital and Harvard Medical School, Boston, MA 02114, USA

<sup>2</sup>Center for Regenerative Medicine, Massachusetts General Hospital and Harvard Medical School, Boston, MA 02114, USA

<sup>3</sup>Steele Laboratory, Massachusetts General Hospital and Harvard Medical School, Boston, MA 02114, USA

### Abstract

The *in vivo* morphology and phenotype of circulating cells that spontaneously contribute to new vessel formation in adults remain unclear. Here, we use high-resolution imaging and flow cytometry to characterize the morphology and phenotype of a distinct population of circulating mononuclear cells contributing to spontaneous new vessel formation after hyperoxic acute lung injury (HALI). We identify a subpopulation of myeloid (CD11b/Mac1<sup>+</sup>) hematopoietic cells co-expressing vascular endothelial growth factor receptor 2 (VEGFR2) and platelet derived growth factor receptor beta (PDGFR $\beta$ ). Moreover, we show that these CD11b<sup>+</sup>VEGFR2<sup>+</sup>PDGFR $\beta$ <sup>+</sup> circulating precursor cells (CPCs) contribute structurally to the luminal surface of capillaries reforming two weeks post-HALI. This indicates that these myeloid CPCs may function, at least transiently, as putative vascular precursors, and has important implications for capillary growth and repair in injury and in pathologies of the lung and other organs.

### Keywords

Hyperoxia; lung capillary injury/restoration; circulating precursor cell

### Introduction

The distal vasculature in the adult lung—distributed through approximately 300,000,000 alveoli—is a major site of injury and remodeling in acute lung injury (ALI). Once destroyed by injury or disease the spontaneous restoration of small vessel and capillary networks, leading to better lung function, has proved limited. While major advances have been made in the treatment and management of patients with ALI, vascular loss remains a significant clinical problem. Moreover, supplemental oxygen levels (>50%) typically administered to improve oxygen delivery to the brain and other vital organs and to peripheral tissues, can exacerbate ventilator-induced lung injury in ALI [1,2]. Similarly, in patients developing radiation pneumonitis, chronic obstructive lung disease, or pulmonary hypertension injury to

Address for correspondence: Rosemary C. Jones, Ph.D., CNY-3416, Building 149, 13<sup>th</sup> Street, Charlestown, MA 02129; phone: (617) 726-4359; fax: (617) 726-4374, rcjones@partners.org; or Dan G. Duda, D.M.D., Ph.D., CNY-3402, Building 149, 13<sup>th</sup> Street, Charlestown, MA 02129; phone: (617) 726-4648; fax (617) 726-1962, duda@steele.mgh.harvard.edu.

the distal lung leading to alveolar disruption and vascular loss is often extensive, and progressive.

New vessel formation during vascular repair in adult organs, previously thought to be limited to sprouting angiogenesis by endothelial cells from nearby vessels, may involve circulating “vasculogenic” cells which have been shown to home to sites of tissue injury and contribute to neovascularization [3]. Blood circulating precursor cells (CPCs) originating from the bone marrow may give rise to endothelial as well as perivascular cells during new vessel formation in tumors or Matrigel plugs [4-7]. While such cells present an attractive target for use in cell-based therapies, it remains currently unclear if CPCs can affect spontaneous vascular growth in lungs. We have shown in an *in vivo* rodent model that pulmonary capillary networks injured in hyperoxia acute lung injury (HALI) spontaneously re-form post-HALI – in a robust, vascular endothelial growth factor (VEGF)-dependent manner [8]. Based on our finding that a population of hematopoietic cells interacts with lung endothelium post-HALI, we hypothesized that they are CPCs that contribute to capillary repair. The goal of this study was to identify the phenotype of these cells by combining high-resolution immunogold labeling with flow cytometric analyses, and determine the role of these CPCs in capillary restoration post-HALI. We show that a population of CD11b<sup>+</sup>VEGFR-2<sup>+</sup>PDGFRβ<sup>+</sup> CPCs interacts with the endothelium of spontaneously re-forming pulmonary capillaries.

## Materials and Methods

### Animals and hyperoxia model of lung capillary injury (HALI) repair model

We used adult male Sprague-Dawley rats (Charles River, Wilmington, MA), after obtaining approval for this protocol from the Subcommittee on Research Animal Care of the Massachusetts General Hospital, Boston, USA. The exposure chamber and the post-HALI neovascularization model used in this study have been described in detail [8,9]. In brief, after weaning from 87% O<sub>2</sub> to 21% O<sub>2</sub> over one week, air breathing over four weeks triggers spontaneous capillary repair: as endothelial cells re-establish patent capillary networks, these markedly increase two weeks post-HALI and by four weeks approach a normal distribution. We collected lung tissue and blood from adult male Sprague-Dawley rats that breathed air (n=19), high oxygen (87%) at normobaric pressure for 4 weeks (HALI, n=13), or high oxygen for four weeks (followed by ~10% less oxygen each day for seven days, week five), and then air for one, two, three or four weeks (post-HALI, n = 11, 13, 8 and 10, respectively). Control rats breathed air alone (n = 15). The distribution of capillaries in the normal lung provided the baseline from which to assess capillary loss after high oxygen and restoration in air.

### Immunocytochemistry

Tissue preparation was performed as previously described [8]. All Unicryl sections were pre-treated with 1% bovine serum albumin (BSA) in PBS (5min at RT), incubated (overnight at 4°C) with (i) mouse anti-rat monoclonal antibody to CD11b (Calbiochem, La Jolla, CA); (ii) rabbit anti-rat polyclonal antibodies to VEGFR2 or PDGFRβ (Calbiochem); or (iii) a rabbit polyclonal antibody to von Willebrand factor (vWF, DAKO, Carpinteria, CA), rinsed in PBS, and incubated (60min at RT) in protein A-gold (pA-AU) (10nm diameter, Auroprobe AG10, Amersham, UK) diluted 1:50 in PBS prior to double-staining. The electron-dense gold particles map antigenic sites for expressed proteins. As a negative control we omitted treatment with the primary antibody and incubated sections in 0.5% BSA in PBS alone: no reactive sites were detected in these control sections.

### Morphologic analyses of CPCs

Using a macro designed to work with NIH Scion (1.62) software (public domain), digital images of capillaries and CPCs were collected and analyzed by TEM via a high sensitivity CCD-300-RC camera (MTI) attached to the 35mm port of the microscope (Advanced Microscopy Techniques Corp., Danvers, MA). We routinely acquired images at  $\times 3,456 - \times 29,623$  magnification. For reference, additional 1-2mm-thick epon-araldite and Unicryl sections were mounted on glass slides, stained with 0.1% toluidine blue: digital images from these sections were collected by brightfield microscopy using a Nikon system (COOLSCOPE CS1, MicroVideo Instruments Inc, Avon, MA), to confirm the sequence of capillary injury and repair (663 representative images).

### Analyses of CPC phenotype

Data for CPC morphology, phenotype and interactions with capillary endothelium during capillary repair were based on high-resolution images of CPCs in HALI (week 4), post-HALI (weeks 6-9) and normal lung (779 CPCs in 1191 capillaries, 2853 images). These images were routinely collected to obtain an overview of capillary endothelial cells and CPCs, to identify apposing and adherent regions of cell membranes, and visualize gold-labeled antigenic sites.

### Phenotypic analyses and kinetic measurements of CPCs by flow cytometry

Blood was collected by cardiac puncture with a 26G needle from rats at two weeks post-HALI and from rats breathing air. Blood cells were stained after their separation from plasma and RBC lysis using ACK lysis buffer (Invitrogen, Carlsbad, CA). We used mouse anti-rat CD31-PE, CD11b-PE and CD45-PE-Cy5 (all from BD Pharmingen, San Jose, CA), and rabbit anti-rat VEGFR2 and PDGFR $\beta$  antibodies (Calbiochem). Immunostaining for VEGFR2 and PDGFR $\beta$  on CPC's surface was performed using a secondary goat anti-rabbit IgG. CPCs were measured on a BD-FACSCalibur system using Cellquest software. The percentage of CPCs was calculated as the fraction of VEGFR2<sup>+</sup> cells among mononuclear cells in peripheral blood. Additionally, VEGFR2<sup>+</sup>CD11b<sup>+</sup> cells were gated and sorted by fluorescence-activated cell sorting. Fifty thousand sorted cells were fixed (in 2% paraformaldehyde in PBS) and centrifuged onto microdissection slides: the cytospin preparations were air-dried, stained with Giemsa, and analyzed by brightfield microscopy. For phenotypic analyses, we labeled rabbit anti-rat VEGFR2 antibodies with Alexa Fluor® 488 and rabbit anti-rat PDGFR $\beta$  antibodies with Alexa Fluor® 647 using Invitrogen labeling kits. Peripheral blood cells were immunostained for CD31, CD11b, CD45, VEGFR2 and PDGFR $\beta$  and the samples were analyzed on an LSR-II cytometer (BD Biosciences). For compensation, we used unstained blood cells and single color controls for each channel.

### Quantitative analysis of CPCs

To estimate the number of capillary CPCs within the lung, we examined a further sample of >200 capillaries at each study time-point (1,077 CPCs in 1,837 capillaries, 3833 images). Starting at an opening at the top of the grid, we systematically collected successive images of all patent/residual capillary units and their associated CPCs in consecutive fields across the (200 mesh) grid face. We collected images from 2 grids per lung and analyzed those fields containing only alveolar-capillary membrane structures, i.e., an occasional field was excluded if a conducting airway, or vessel, was also present. CPC number per lung was estimated from the average number of cells per microscopic field, volume of tissue per field and total lung volume (total cells in the lung =  $V_L/H_C \times C_S/A_S \times 200 / N_R \times (10^4 \text{cm})^3/\text{cm}^3$ , where  $V_L$  = total lung volume,  $H_C$  = average height of cell,  $C_S$  = number of cells counted in the grid,  $A_S$  = surface area of grid ( $\pi r^2$ ),  $N_R$  = number of grid openings with capillary

tissue). A subset of these data further demonstrated the proportion of CPCs adherent to capillary endothelium.

## Results

### Capillary segments injured in HALI spontaneously repair post-HALI

We studied the CPCs at time-points that correspond to phases of capillary injury in HALI and active repair post-HALI (Figure 1a). At these time points, the alveolar-capillary membrane was characterized by endothelial loss/avascular zones in HALI, and by restored capillary networks post-HALI reminiscent of the open (lace-like) networks in normal lungs (Figure 1b-d). Endothelial cell injury, frequent in both patent and residual capillary structures in HALI, was infrequent post-HALI, suggesting initial sloughing of injured endothelial cells and later expansion of endothelial surfaces by local or by circulating precursors.

### CPC have a distinct morphology and are numerous in normal lung, in HALI and post-HALI

We identified CPCs as a morphologically distinct mononuclear cell population in the normal lung, in HALI and in post-HALI (Figure 2) – monocytic cells of approximately 9 $\mu$ m (maximum) diameter, with a high nucleus to cytoplasm ratio, and a cytosol characterized by abundant free ribosomes and large mitochondria. The cells were distinct from capillary endothelial cells and from mature intravascular hematopoietic cells circulating through the lung (e.g. granulocytes, eosinophils, mast cells and monocytes, see Supplementary Figure S1). CPCs rarely interacted with capillary walls in normal lung (9% of CPCs), suggesting that the vast majority were freely circulating. However, CPCs were trapped in narrowed capillaries in HALI, 35% of the population interacted with endothelial cells early in the post-HALI phase (weeks 6 and 7), but not at later time-points (6% at weeks 8 and 9). CPCs formed a significant intravascular population (i.e., estimated at approximately 5-8 million cells/lung) at all of the time-points evaluated in this study.

### A subset of blood CPCs expresses CD11b, VEGFR2, and PDGFR $\beta$ on cell surface

By flow cytometric analysis, in post-HALI (week 8) we found that a subset of mononuclear cells (approximately 0.5%) co-express the endothelial-selective marker VEGFR2 and the mesenchymal-selective marker PDGFR $\beta$  in peripheral blood (Figure 3a-f). The scattering properties of these cells, consistent with the morphology of CPCs, were similar to those of lymphocytes. Of interest, all VEGFR2<sup>+</sup>PDGFR $\beta$ <sup>+</sup> cells expressed CD45 and CD31, and some expressed the myeloid-cell associated integrin CD11b (Mac1) on their surface (Figure 3e). Cytospin preparations of VEGFR2<sup>+</sup> cells revealed the same monocytic morphology as CPCs in tissue sections. VEGFR2<sup>+</sup>CD45<sup>+</sup> CPCs represented 1-2% of the circulating mononuclear cells, at all of the time-points evaluated in this study.

### CPCs detected in lung capillaries are CD11b<sup>+</sup>VEGFR2<sup>+</sup>PDGFR $\beta$ <sup>+</sup>

Next, by high-resolution imaging and immunogold labeling of lung tissue, we detected antigenic sites for the VEGFR2 on all intravascular CPCs (Figure 4a). Further analysis showed that these CPCs expressed PDGFR $\beta$  (Figure 4b). Moreover, analysis of CPCs in serial sections demonstrated co-expression of VEGFR2 and PDGFR $\beta$  (Figure 4c,d). Furthermore, these CPCs stained positively for CD11b with similar cytoplasmic patterns of staining as compared to other myeloid-lineage cells (e.g., eosinophils and PMNs)(Figure 4e). Finally, these CPCs expressed the endothelial marker vWF (Figure 4f).

## CPCs participate in lung capillary restoration post-HALI

To study the interaction between CPCs and the endothelium of re-forming capillaries, we reconstructed (from sets of ~20-25 serial high resolution digital images) single CPCs and adjacent endothelial cells from ~90 capillary segments forming during the height of the regenerative response post-HALI (after 1-2 weeks). Attaching first focally to the endothelial apical plasmalemmal membrane via multiple small cytoplasmic extensions (Supplementary Figure S2), CPCs aligned with endothelial surfaces and, in regions, became adherent, i.e., the two cells were no longer delineated by intact plasmalemmal membranes (Figure 5a-d). They adhered to endothelial cells with normal morphology and not to injured (oncotic, necrotic, apoptotic) endothelial cells. CPCs and endothelial cells were judged adherent by loss of integrity of the two plasmalemmal membranes (Figure 5b-d). This is in contrast to inflammatory hematopoietic cells transiting endothelium cells via diapedesis, where each cell type clearly retains an intact plasmalemmal membrane. We did not observe inflammatory cell infiltration or adherence between CPCs in the lungs during or post-HALI.

The insertion of CPC processes between endothelial cells indicated their retention within the capillary luminal surface (Figure 6a,b). At this transitional stage, the CPCs were still clearly identified from endothelial cells by morphology. All the cells forming a contiguous capillary surface, however, displayed characteristic endothelial morphology. Nevertheless, the cells forming the capillary surfaces expressed focal accumulations of CD11b antigenic sites, typical of CPCs (Figure 6c). In a non-biased sample of endothelial cells in the early post-HALI phase, approximately 32% of them (33/103 nucleated endothelial cells) were CD11b<sup>+</sup>.

Rare CPCs were present post-HALI in the interstitium of the alveolar-capillary membrane (after transit from the capillary lumen and across endothelium), where they aligned as CD11b<sup>+</sup> perivascular cells (Supplementary Figure S3). They were identified by their morphology from interstitial fibroblasts, which are the major source of PDGFR $\beta$ <sup>+</sup> perivascular cells developing around small vessels in the alveolar-capillary membrane in this model [10,11].

## Discussion

We have characterized by morphology and phenotype a novel population of CPCs in normal lung, in HALI and post-HALI; and demonstrated the interaction of these cells with capillary endothelium re-forming after injury. Other studies have failed to detect any contribution by *bona fide* endothelial CPCs to the extensive vascular growth and remodeling that occurs in a model of regenerative lung growth [12]. Cells identified as vascular progenitors have been identified in the pulmonary arteries of patients with chronic obstructive pulmonary disease, however, where they contribute to capillary repair and pulmonary vascular remodeling [13]. In line with this, and our present findings, studies in parabiotic mice (GFP<sup>+</sup> mice and wild mice with a co-joined circulation) demonstrated that GFP<sup>+</sup> cells derived from the circulation are retained in pulmonary tissue following injury [14]. In addition, Balasubramaniam and colleagues reported that circulating BMD cells are necessary to maintain vascular density in the developing and adult mouse lung challenged by hyperoxia [15]. Several groups have demonstrated a direct interaction between CPCs—including VEGFR2<sup>+</sup> or PDGFR $\beta$ <sup>+</sup> myeloid cells—and blood vessels in tumors [16,17]. In addition, myeloid growth factor over-expression has been shown to protect lung capillaries during HALI [18].

Here, we characterize a previously undescribed CPC population of VEGFR2<sup>+</sup>PDGFR $\beta$ <sup>+</sup> cells, expressing hematopoietic markers, and morphologically distinct from mature hematopoietic cells. Our data highlight a role for this CPC population in the luminal and abluminal surfaces of capillaries re-forming in the adult lung post-HALI. Only cells with CPC morphology were identified interacting with capillary walls, and these cells expressed



detectable levels of CD11b, VEGFR2 and PDGFR $\beta$ . Furthermore, at this time of increased capillary repair, the absence of monocyte/monocytic or PMN cell infiltrates in the lung's interstitium indicated the absence of an overt inflammatory response.

Our data support the adhesion of myeloid VEGFR2<sup>+</sup>PDGFR $\beta$ <sup>+</sup> CPCs to capillary endothelial cells early in the post-HALI phase, and indicate that these cells integrate into the capillary surface. Since the CPCs studied by us were not genetically marked, their progeny could not be defined morphologically at later time-points. Thus, in this model we cannot discern whether the CPCs eventually “differentiate” into endothelial cells with a “mature” (i.e., non-hematopoietic) phenotype. Nor can we detect if the vascular CPCs are replaced by local-derived, proliferating lung capillary endothelial or perivascular cells. Future studies should determine if CPCs are only transiently incorporated into the vessels or, conversely, if they “differentiate” into mature capillary endothelial and/or perivascular cells. The CPCs identified in the lung tissue studies (by intracellular detection of the two proteins) express both VEGFR2 and PDGFR $\beta$  at some level, and only cells with these markers interact with endothelium. Thus, VEGFR2 and PDGFR $\beta$  expression could not be used to discriminate between CPCs aligning as endothelial or perivascular cells. Moreover, endothelial cells may express PDGFR $\beta$  [19] and conversely, perivascular cells may express VEGFR2 [20].

A greater understanding of these cells, including the molecular mechanisms mediating the vascular responses reported here, might improve therapeutic strategies to address vascular loss following injury or disease in the lung and other organs. Future work should determine if CPCs could be used/engineered to promote capillary restoration in the developing or adult lung. Moreover, it will be critical to establish if VEGFR2<sup>+</sup>PDGFR $\beta$ <sup>+</sup> CPCs have any relevance for other types of physiological and pathological capillary formation in adults, such as occurs in tumors, wounds and ischemic tissues.

## Supplementary Material

Refer to Web version on PubMed Central for supplementary material.

## Acknowledgments

The work of the authors is supported by grants from the NIH (R01-HL070866, R01-HL089252, R01-CA115767, P01-CA80124, R01-CA85140 and R01-CA126642).

## References

1. Dos Santos CC. Hyperoxic acute lung injury and ventilator-induced/associated lung injury: new insights into intracellular signaling pathways. *Crit Care*. 2007; 11(2):126. [PubMed: 17466082]
2. Li LF, Liao SK, Ko YS, Lee CH, Quinn DA. Hyperoxia increases ventilator-induced lung injury via mitogen-activated protein kinases: a prospective, controlled animal experiment. *Crit Care*. 2007; 11(1):R25. [PubMed: 17316425]
3. Rafii S, Lyden D. Therapeutic stem and progenitor cell transplantation for organ vascularization and regeneration. *Nat Med*. 2003 Jun; 9(6):702–12. [PubMed: 12778169]
4. Du R, Lu KV, Petritsch C, et al. HIF1 $\alpha$  induces the recruitment of bone marrow-derived vascular modulatory cells to regulate tumor angiogenesis and invasion. *Cancer Cell*. 2008 Mar; 13(3):206–20. [PubMed: 18328425]
5. Rafii S, Lyden D, Benzra R, Hattori K, Heissig B. Vascular and haematopoietic stem cells: novel targets for anti-angiogenesis therapy? *Nat Rev Cancer*. 2002 Nov; 2(11):826–35. [PubMed: 12415253]
6. Rajantie I, Ilmonen M, Alminaita A, Ozerdem U, Alitalo K, Salven P. Adult bone marrow-derived cells recruited during angiogenesis comprise precursors for periendothelial vascular mural cells. *Blood*. 2004 Oct 1; 104(7):2084–6. [PubMed: 15191949]

7. Anghelina M, Krishnan P, Moldovan L, Moldovan NI. Monocytes/macrophages cooperate with progenitor cells during neovascularization and tissue repair: conversion of cell columns into fibrovascular bundles. *Am J Pathol.* 2006 Feb; 168(2):529–41. [PubMed: 16436667]
8. Jones R, Capen D, Cohen KS, Munn LL, Jain RK, Duda DG. A protocol for a lung neovascularization model in rodents. *Nat Protoc.* 2008; 3(3):378–87. [PubMed: 18323809]
9. Jones R, Capen D, Cohen KS, Munn LL, Jain RK, Duda DG. A protocol for phenotypic detection and characterization of vascular cells of different origins in a lung neovascularization model in rodents. *Nat Protoc.* 2008; 3(3):388–97. [PubMed: 18323810]
10. Jones R. Ultrastructural analysis of contractile cell development in lung microvessels in hyperoxic pulmonary hypertension. Fibroblasts and intermediate cells selectively reorganize nonmuscular segments. *Am J Pathol.* 1992 Dec; 141(6):1491–505. [PubMed: 1466406]
11. Jones R, Capen D, Jacobson M. PDGF and microvessel wall remodeling in adult lung: imaging PDGF-Rbeta and PDGF-BB molecules in progenitor smooth muscle cells developing in pulmonary hypertension. *Ultrastruct Pathol.* 2006 Jul-Aug; 30(4):267–81. [PubMed: 16971352]
12. Ziegelhoeffer T, Fernandez B, Kostin S, et al. Bone marrow-derived cells do not incorporate into the adult growing vasculature. *Circ Res.* 2004 Feb 6; 94(2):230–8. [PubMed: 14656934]
13. Peinado VI, Ramirez J, Roca J, Rodriguez-Roisin R, Barbera JA. Identification of vascular progenitor cells in pulmonary arteries of patients with chronic obstructive pulmonary disease. *Am J Respir Cell Mol Biol.* 2006 Mar; 34(3):257–63. [PubMed: 16239642]
14. Abe S, Boyer C, Liu X, et al. Cells derived from the circulation contribute to the repair of lung injury. *Am J Respir Crit Care Med.* 2004 Dec 1; 170(11):1158–63. [PubMed: 15282197]
15. Balasubramaniam V, Mervis CF, Maxey AM, Markham NE, Abman SH. Hyperoxia reduces bone marrow, circulating, and lung endothelial progenitor cells in the developing lung: implications for the pathogenesis of bronchopulmonary dysplasia. *Am J Physiol Lung Cell Mol Physiol.* 2007 May; 292(5):L1073–84. [PubMed: 17209139]
16. Conejo-Garcia JR, Benencia F, Courreges MC, et al. Tumor-infiltrating dendritic cell precursors recruited by a beta-defensin contribute to vasculogenesis under the influence of Vegf-A. *Nat Med.* 2004 Sep; 10(9):950–8. [PubMed: 15334073]
17. Song S, Ewald AJ, Stallcup W, Werb Z, Bergers G. PDGFRbeta+ perivascular progenitor cells in tumours regulate pericyte differentiation and vascular survival. *Nat Cell Biol.* 2005 Sep; 7(9):870–9. [PubMed: 16113679]
18. PaineR3rdWilcoxonSEMorrisSBTransgenic overexpression of granulocyte macrophage-colony stimulating factor in the lung prevents hyperoxic lung injury. *Am J PatholAm J Pathol*2003Dec16362397406 [PubMed: 14633611]
19. Jones R, Capen D, Jacobson M, Munn L. PDGF and microvessel wall remodeling in adult rat lung: imaging PDGF-AA and PDGF-Ralpha molecules in progenitor smooth muscle cells developing in experimental pulmonary hypertension. *Cell Tissue Res.* 2006 Dec; 326(3):759–69. [PubMed: 16794827]
20. Greenberg JI, Shields DJ, Barillas SG, et al. A role for VEGF as a negative regulator of pericyte function and vessel maturation. *Nature.* 2008 Dec 11; 456(7223):809–13. [PubMed: 18997771]





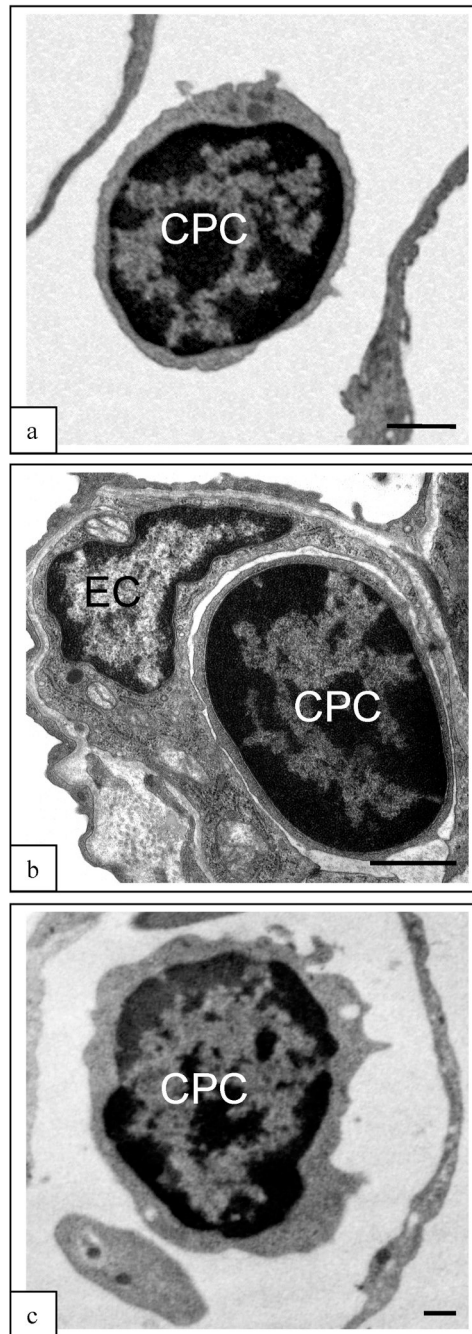


**Figure 2. CPC in capillaries of normal lung, in HALI and post-HALI**

CPC were identified by their similar morphology as freely circulating cells in patent capillaries of normal lung (a), in the narrowed capillary segments in HALI (b), and again as freely circulating cells in patent capillary segments post-HALI (c, week 9). Characterized by a high ratio of nucleus to cytoplasm and dense arrangement of heterochromatin CPCs were clearly identified from adjacent capillary endothelial cells (see b). The CPC illustrated in (b) differs in morphology from the adjacent endothelial cell (EC) forming the capillary wall. 80nm-thick epon resin sections stained with uranyl acetate and lead citrate. Bars = 1 $\mu$ m (a-c).

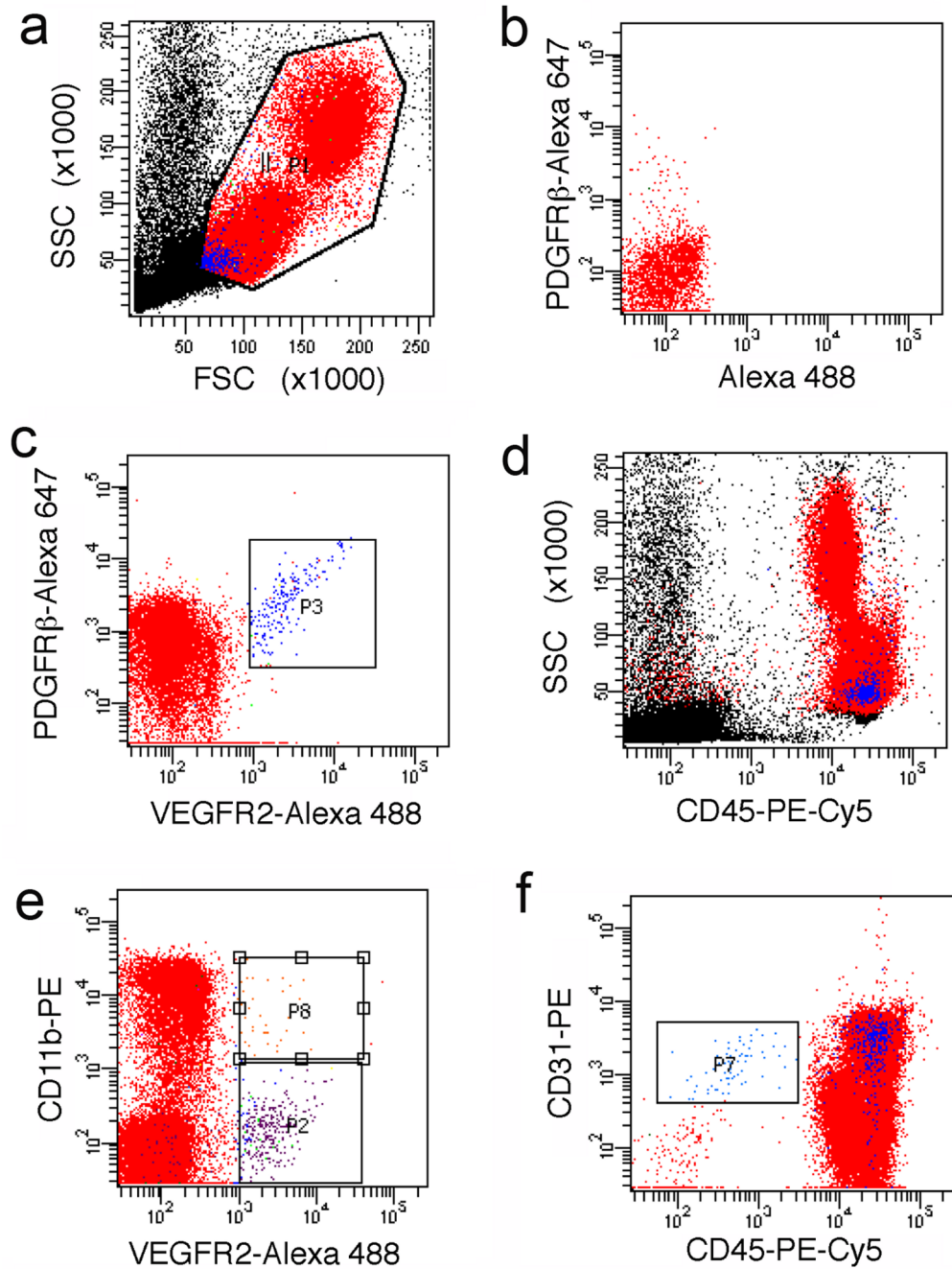


**Figure 3. Phenotypic characterization of circulating precursor cells (CPCs)**

LSR-II flow cytometric analyses of (gated, **a**) mononuclear cells in peripheral blood, identified a distinct population of CPCs that co-express VEGFR2 and PDGFR $\beta$  (**c**); single-color controls were used for compensation (e.g., see staining for PDGFR $\beta$ -Alexa Fluor 647 in **b**). These CPCs (in blue) are positive for CD45 (**d**) and show scattering properties typical of small cells with a high nucleus to cytoplasm ratio (**a**, **d**). A subset of CPCs is positive for CD11b (**e**), whereas all VEGFR2<sup>+</sup>PDGFR $\beta$ <sup>+</sup> CPCs are positive for CD31 (**f**); CPCs are distinct from cells with a phenotype consistent with “circulating endothelial cells”, i.e., CD31<sup>+</sup>CD45<sup>-</sup> (in red gate in **f**).

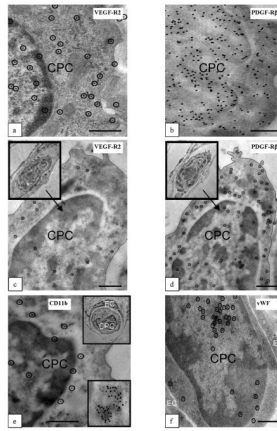


**Figure 4. Phenotypic characterization of CPCs in lungs post-HALI**

Antigenic sites, visualized with 10nm protein A-gold by high-resolution microscopy, demonstrated that CPCs were VEGFR2<sup>+</sup> (a) and PDGFRβ<sup>+</sup> (b) post-HALI (weeks 6 and 7). Representative images of the same CPC profile in adjacent sections of lung tissue (c and d, and insets) demonstrated co-expression of VEGFR2 and PDGFRβ antigenic sites post-HALI (week 7). Representative images of antigenic sites expressed by CPCs post-HALI (week 7): CD11b (e and inset) and for vWF (f). Typically, the sites for CD11b were uniformly distributed over CPCs but also appeared as clusters (e, see bottom inset, illustrating an example of a cluster of ~40 CD11b<sup>+</sup> labeled sites). 10nm gold-labeled antigenic sites (a, c-f) are circled for clarity to distinguish these from 7-8nm ribosomes on cell profiles. 90nm-thick Unicryl resin sections stained with uranyl acetate and lead citrate. Bars = 0.5μm (a-f).

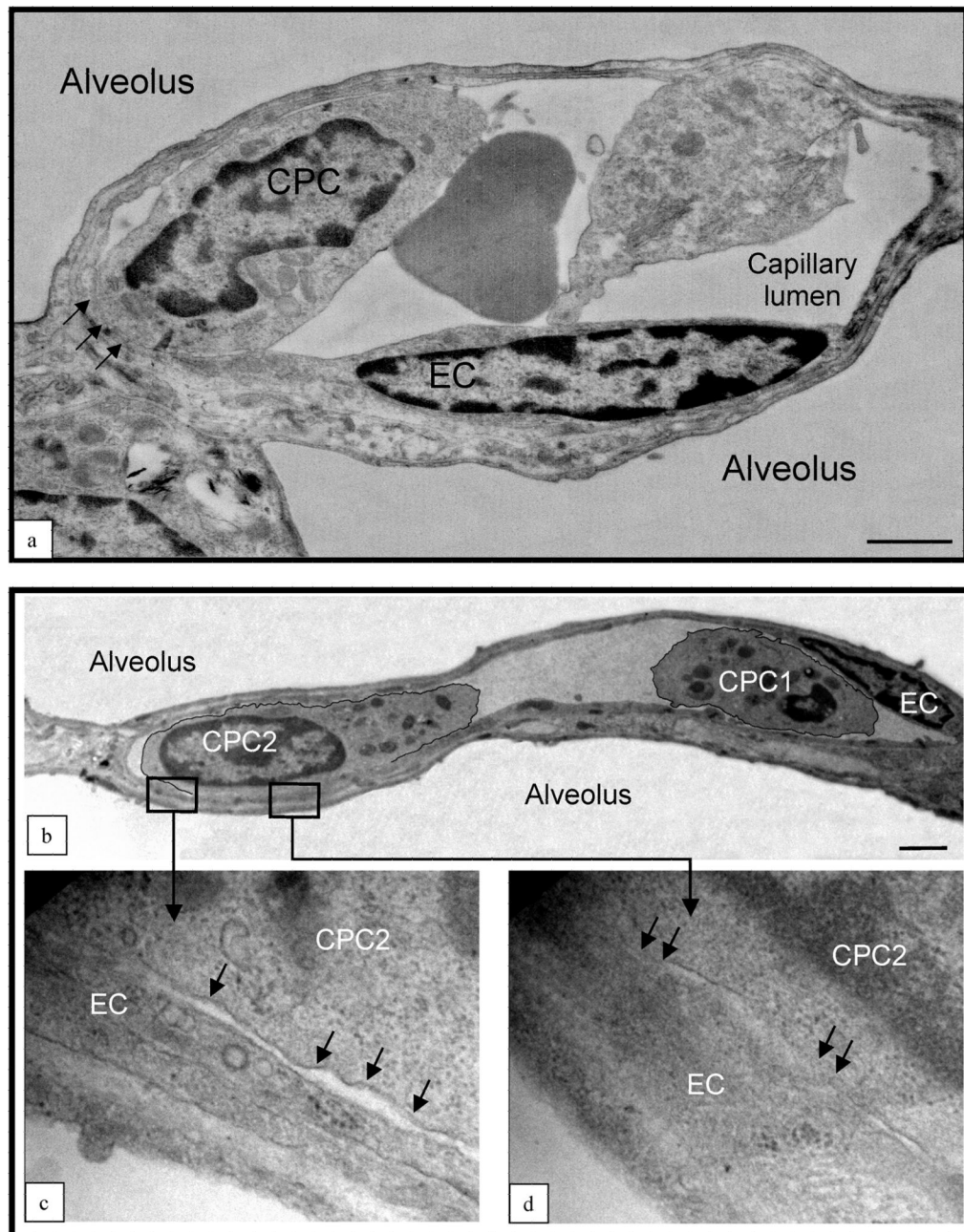


**Figure 5. CPCs contact and adhere to endothelium post HALI**

(a) Representative image of CPC aligning and adhering to a capillary endothelial cell (EC, see arrows) post-HALI (week 7). At this time approximately 35% of CPCs form contacts with lung capillary endothelial cells. (b) Representative image of two CPCs in a lung capillary post-HALI (week 6): CPC1 appears free in the lumen and CPC2 is in the process of adhering to the adjacent endothelial cell (see boxed areas): higher magnification shows regional separation of two distinct cell membranes (lower left image, arrows), and regional loss of membrane delineation between the two cells (lower right image, arrows). 80nm-thick epon resin sections stained with uranyl acetate and lead citrate. Bars = 1 $\mu$ m (a) and 2 $\mu$ m (b).



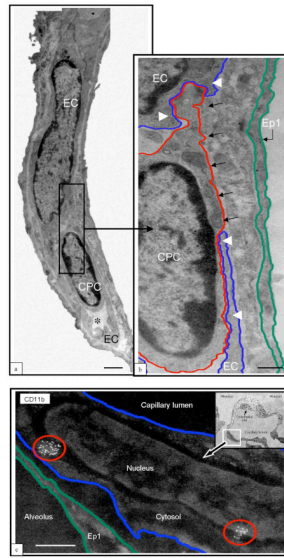


**Figure 6. CD11b<sup>+</sup> CPCs and cells integrate into capillary surfaces post HALI**  
 Illustrations of CPC (a) and capillary endothelial cell (EC) in a residual capillary structure post-HALI (week 6). An asterisk marks the restricted capillary lumen at this time. A region of the CPC cytosol is inserted between the processes of two capillary endothelial cells (b, arrows). Note the location of the CPC within the capillary lumen in relation to the processes of adjacent endothelial cells, to (an un-delineated) perivascular cell process, and to the underlying epithelial (Ep1) cell process. The blue line delineates the plasmalemmal membrane of the capillary endothelial cell, the red line outlines the CPC, and the green line demarcates the adjacent epithelial type 1 (Ep1). (c) Representative image of lung capillary (see boxed area of inset) and higher magnification of the luminal surface illustrating cell clusters of antigenic sites for CD11b (circled in red) typical of CPCs expressing this protein post-HALI (week 7). Image is inverted to highlight the location of this cell with antigenic sites. The other endothelial cell indicated in the same capillary (see inset, small arrow) does not express CD11b. 80nm-thick epon resin section (a,b), and 90nm-thick Unicryl resin section (c), stained with uranyl acetate and lead citrate. Bars =1 $\mu$ m (a), 0.5 $\mu$ m (b,c).